lineaments hundreds of kilometers long and interpreted to be scarps and faults are arrayed generally radially around the corona, and there is a particularly well-developed trend of lineaments in the northeast-southwest direction that extends to the northeast in a linear belt toward Western Aphrodite Terra. The characteristics of Lada Terra (linear deformed zones of probable extensional origin, coronae) are quite different from those of the northern high-latitude highland, Ishtar Terra (compressional mountain belts, steep bounding slopes, and abundant tessera terrain), but in many respects they are similar to the characteristics of the cluster of coronae seen in Mnemosyne Regio, to the west of Ishtar Terra (*21*).

A total of 49 features of possible impact origin have been mapped in this region. The craters tend to be concentrated in the plains rather than in the uplands-highlands, opposite to the trend in the Beta-Eistla region (*11, 22*). The density of craters observed in the region mapped in Fig. 1 (55.6 × 10^6 km^2) is 0.88 crater per 10^6 km^2, similar to the 0.92 per 10^6 km^2 seen in the Beta-Eistla region (*22*) and less than that observed for the northern high-latitude Venera coverage (1.3 per 10^6 km^2). This density indicates that the age of this region is similar to the age (250 to 1000 million years) interpreted for the northern high latitudes (*2, 3*). Adding this part of the southern hemisphere (12% of the surface of Venus) to that previously dated brings the total area estimated to have formed during the last 20% of the history of the planet to approximately 43%.

Of the three types of deformation outlined by Basilevsky *et al.* (*5*) in the Venera coverage (beltlike, circular, areal), linear beltlike deformation appears to dominate this region; the lineament belts of Themis and Lada Terrae occupy many thousands of kilometers and extend out of the region to connect with major tectonic zones elsewhere. These belts are interpreted to be of extensional origin, whereas the additional lineament belts mapped in Lavinia Planitia are interpreted to be of compressional origin. Orogenic belts such as those surrounding Lakshmi Planum (*6*) are not observed. Circular deformation is common in the form of abundant corona-like features associated with the linear deformation belts of Lada and Themis and in the isolated coronae of Lada Terra. Areal deformation is well developed only in Alpha Regio and is not as abundant as in the Venera coverage, although additional tessera may underlie the plains, particularly around Alpha Regio. Plains units of apparent volcanic origin are common, and the style of plains volcanism is similar to that seen elsewhere (*4, 5, 11*). Large volcanic edifices are commonly associated with topographic rises (Ushas-Hathor trend) or linear belt deformation (Themis and northern Lada Terra).

One of the most distinctive characteristics of the mapped region is the presence and abundance of the linear deformation zones with associated corona-like features. These zones further delineate the presence of regional and global zones of upwelling and extension, and the different scales of corona-like features provide evidence for different scales of mantle instabilities and upwelling. The Magellan mission (*23*) will provide complementary viewing geometry and higher resolution imaging and altimetry data so that more detailed characteristics and relations among these basic units can be determined.

REFERENCES AND NOTES

1. G. H. Pettengill *et al.*, *J. Geophys. Res.* **85**, 8261 (1980); H. Masursky *et al.*, *ibid.*, p. 8232.
2. B. A. Ivanov *et al.*, *ibid.* **91**, D413 (1986); A. T. Basilevsky *et al.*, *ibid.* **92**, 12869 (1987).
3. G. G. Schaber *et al.*, *Astron. Vestn.* **21**, 144 (1987).
4. V. L. Barsukov *et al.*, *J. Geophys. Res.* **91**, D378 (1986); A. L. Sukhanov *et al.*, *U.S. Geol. Surv. Misc. Geol. Invest. Map I-2059* (1989).
5. A. T. Basilevsky *et al.*, *J. Geophys. Res.* **91**, D399 (1986).
6. L. S. Crumpler *et al.*, *Geology* **14**, 1031 (1986); J. W. Head, *ibid.* **18**, 99 (1990).
7. D. Senske, *Earth Moon Planets* **50**, 305 (1990); R. Arvidson *et al.*, *Proc. Lunar Planet. Sci. Conf.* **20**, 557 (1990).
8. G. G. Schaber, *Geophys. Res. Lett.* **9**, 499 (1982).
9. G. E. McGill *et al.*, *ibid.* **8**, 737 (1981); E. R. Stofan *et al.*, *Geol. Soc. Am. Bull.* **101**, 143 (1989).
10. J. W. Head III and L. S. Crumpler, *Science* **238**, 1380 (1987).
11. D. B. Campbell *et al.*, *ibid.* **246**, 373 (1989).
12. A circularly polarized signal was transmitted, and the results we describe are based on images derived from the expected, single-scatter sense of received circular polarization. Incidence angles varied from about 10° to 78°. The signal-to-noise ratio decreases with increasing incidence angle because the backscatter cross section decreases and atmospheric absorption increases. For the area from 12° to 60°S 25 "looks" (estimates of the backscatter cross section) were averaged, and from 60° to 78°S 16 looks were averaged to form the images.
13. E. Stofan and J. Head, *Lunar Planet. Sci.* **XVI**, 825 (abstr.) (1985); E. Stofan *et al.*, *ibid.* **XXI**, 1210 (abstr.) (1990).
14. D. A. Senske and J. W. Head, *ibid.* **XX**, 984 (abstr.) (1989).
15. E. Stofan *et al.*, *ibid.* **XXI**, 1208 (1990).
16. D. Bindschadler *et al.*, *Geophys. Res. Lett.* **17**, 171 (1990).
17. D. Bindschadler and J. Head, *J. Geophys. Res.*, in press.
18. S. Keddie *et al.*, *Lunar Planet. Sci.* **XXI**, 615 (abstr.) (1990).
19. S. L. Frank and J. W. Head, *Earth Moon Planets* **50**, 421 (1990).
20. E. Stofan and A. Pronin, *Icarus* **87**, 452 (1990).
21. E. Stofan and J. Head, *ibid.* **83**, 216 (1990).
22. D. Campbell *et al.*, *Geophys. Res. Lett.* **17**, 1389 (1990).
23. R. S. Saunders *et al.*, *J. Geophys. Res.* **95**, 8339 (1990).
24. The National Academy and Ionosphere Center is operated by Cornell University under a cooperative agreement with the National Science Foundation and with support from the National Aeronautics and Space Administration (NASA). Supported under grants from the Planetary Geology and Geophysics Program and the Planetary Astronomy Program of the Solar System Exploration Division of NASA to D.B.C. and J.W.H. We thank the personnel at the Arecibo Observatory for help and discussions with E. Stofan, S. Keddie, S. Frank, and A. deCharon are gratefully acknowledged.

6 August 1990; accepted 23 October 1990

Atomic-Resolution Electrochemistry with the Atomic Force Microscope: Copper Deposition on Gold

S. Manne, P. K. Hansma, J. Massie, V. B. Elings, A. A. Gewirth*

The atomic force microscope (AFM) was used to image an electrode surface at atomic resolution while the electrode was under potential control in a fluid electrolyte. A new level of subtlety was observed for each step of a complete electrochemical cycle that started with an Au(111) surface onto which bulk Cu was electrodeposited. The Cu was stripped down to an underpotential-deposited monolayer and finally returned to a bare Au(111) surface. The images revealed that the underpotential-deposited monolayer has different structures in different electrolytes. Specifically, for a perchloric acid electrolyte the Cu atoms are in a close-packed lattice with a spacing of 0.29 ± 0.02 nanometer (nm). For a sulfate electrolyte they are in a more open lattice with a spacing of 0.49 ± 0.02 nm. As the deposited Cu layer grew thicker, the Cu atoms converged to a (111)-oriented layer with a lattice spacing of 0.26 ± 0.02 nm for both electrolytes. A terrace pattern was observed during dissolution of bulk Cu. Images were obtained of an atomically resolved Cu monolayer in one region and an atomically resolved Au substrate in another in which a 30° rotation of the Cu monolayer lattice from the Au lattice is clearly visible.

WE REPORT ATOM-RESOLVED AFM images (*1, 2*) of bulk and underpotential-deposited Cu on a Au surface in two different electrolytes. Underpotential deposition (upd) is an electrochemical process in which one to several monolayers or submonolayers of a foreign adatom are deposited on a surface at potentials positive from the reversible Nernst potential. The upd process on noble metal surfaces has attracted substantial attention (*3*) over the past two decades because it may be important in all deposition processes and because upd-modified surfaces show increased resistance to poisoning from oxidation products, making these surfaces potentially attractive for use in fuel cells and in sensors (*4*). Direct knowledge of the monolayer structure is important in order to evaluate the factors giving rise to the underpotential shift and to determine the origins of the distinctive properties of these monolayers.

An archetype of the upd process is Cu on Au, which has been extensively studied because of the inertness of the Au electrode and the ease of its preparation. Kolb and co-workers (*5*) have developed ultrahigh vacuum (UHV)–based techniques to study this system that involve removing the electrode from solution into clean environments. However, removing the electrode may alter the structure of the overlayer and make correlation with the electrochemistry uncertain.

Direct in situ measurements on the Cu on Au upd process have been of two types. Surface x-ray absorption fine structure (EXAFS) has been used (*6*) to obtain distances between Cu atoms in the overlayer and the Au substrate and between neighboring Cu atoms. Second, Kolb, Behm, and co-workers (*7*) recently used scanning tunneling microscopy (STM) to determine the structure of Cu monolayers on Au(111) and Au(100) surfaces in sulfate electrolyte. We confirmed their Au(111) results and extended the imaging to the complete electrochemical cycle in two electrolytes. We show that a change between two ostensibly noncomplexing electrolytes can strongly affect the structure and energetics of the upd process.

The AFM used in these experiments was a commercially available model (*8*) that is based on designs described elsewhere (*9–12*). A fluid cell made from glass (Fig. 1) was used to hold the electrolyte (~0.5 ml) (*13*). Cyclic voltammetry of Cu upd onto Au in perchlorate electrolyte showed (*14*) one desorption peak at +0.33 V, while in sulfate two peaks were observed at +0.21 and +0.05 V (*15*).

AFM images in either electrolyte taken at +0.7 V (Fig. 2A) prior to Cu deposition showed large areas exhibiting Au(111) atomic resolution. We have reported this result previously in pure water without potential control (*16*). The xy motion of the translator was calibrated by setting the atom-atom distance of the observed Au(111) lattice to the known value of 0.29 nm. It is, however, somewhat surprising that this corrugation should be seen at all in sulfuric acid electrolyte, since radiochemical data (*17, 18*) indicate that there should be substantial sulfate adsorbed onto the electrode surface at these potentials. That this is not seen here implies that either the sulfate is not as strongly adsorbed as was previously supposed or that the AFM is capable of sweeping away bound electrolyte. Finally, these atomic-resolution images are stable for long periods (>1 hour) of time, which suggests that chloride contamination from the perchlorate electrolyte is not significant in our experiment. [STM images have been greatly destabilized by chloride concentrations as small as 10^{-5} M (*19*).]

Sweeping the potential to −0.100 V at 10 mV/s to initiate bulk Cu deposition onto the Au(111) surface resulted in a series of disordered scans that quickly (10 s) settled into images (Fig. 2B) of a close-packed surface with an atom-atom distance of 0.26 ± 0.02 nm. We associate these features with a Cu(111) surface formed atop the Au(111) substrate in the course of bulk deposition. We were able to obtain stable views of this relatively reactive surface for several minutes without observing evidence of oxidation of the surface. In air, Cu oxidizes quickly and atomic-resolution images with the STM have only been obtained in UHV environments (*20*). That the Cu surface can be made stable in electrochemical environments for atomic-resolution scanning suggests that it may be possible to use this substrate for binding different anions.

Sweeping the potential to +0.110 V removed the bulk-deposited Cu but left the upd monolayer in place. Here, different images were found in the two different electrolytes. In perchloric acid, images (Fig. 2C) appeared with the same spacing (0.29 ± 0.02 nm) found for the Au(111) surface at +0.7 V. However, the lattice direction was rotated 30° ± 10° relative to the underlying Au lattice, whose orientation was previously established and had the same orientation as the bulk deposited Cu (*21*). Hence, the Cu adatoms are arranged in a close-packed layer on top of the Au lattice but the 30° rotation suggests that the overlayer is incommensurate with the Au(111) surface (Fig. 2D). As the covalent radius of the Cu atoms is somewhat greater than that of Au (0.175 versus 0.142 nm), one would expect some strain to be present in a commensurate close-packed overlayer structure, which may be the origin of the incommensurate structure that we find here.

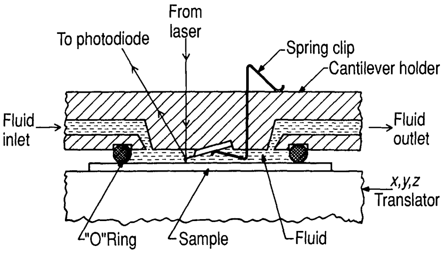

Fig. 1. Cross section of the fluid cell used for electrochemistry.

In sulfuric acid electrolyte, a completely different overlayer structure was found. At +0.100 V, we observed (Fig. 2E) a spacing of 0.49 ± 0.02 nm with a 30° ± 10° rotation relative to the underlying Au lattice. This is equivalent to a $(\sqrt{3} \times \sqrt{3})R30°$ overlayer structure (Fig. 2F) and, as such, is substantially more open than the close-packed structure found for the perchlorate. The $(\sqrt{3} \times \sqrt{3})R30°$ structure was also found with the STM (*7*) and has been suggested by studies of electrodes that were removed from solution (*5, 14*).

Finally, sweeping the potential back to +0.7 V removes the overlayer and leaves the clean Au(111) surface with a structure identical to that shown in Fig. 2A. In studies of electrodes that have been removed from solution, it has been suggested (*14*) that the Au electrode structure is changed after a cycle through the upd process. We find no such evidence of any change here, and it appears that upd of Cu onto Au(111) in either electrolyte is a completely reversible process. Repeating the electrochemical cycle gave results identical to the first sweep.

Two surprises came during this work. First, images obtained during the bulk Cu dissolution in perchlorate electrolyte (at approximately −0.05 V) revealed a terrace pattern, a monolayer step from which is shown in Fig. 3A. Similar images were observed in sulfate. These images suggest that the dissolution of Cu occurs at multiple step edges that must remove the Cu from multiple layers of the bulk. Etching processes have not been observed previously in redox-active electrolyte with atomic resolution. The etching continued until only the upd monolayer remained.

The second surprise came at a potential of +0.144 V in sulfate (Fig. 3B). Here, the upper half of the image shows the upd monolayer, and the lower part exhibits the characteristic Au(111) corrugation. The height of the step between these two areas

---

S. Manne and P. K. Hansma, Department of Physics, University of California, Santa Barbara, Santa Barbara, CA 93106.
J. Massie and V. B. Elings, Digital Instruments, 6780 Cortona Drive, Santa Barbara, CA 93117.
A. A. Gewirth, School of Chemical Sciences, University of Illinois, Urbana, IL 61801.

---

*To whom correspondence should be addressed.

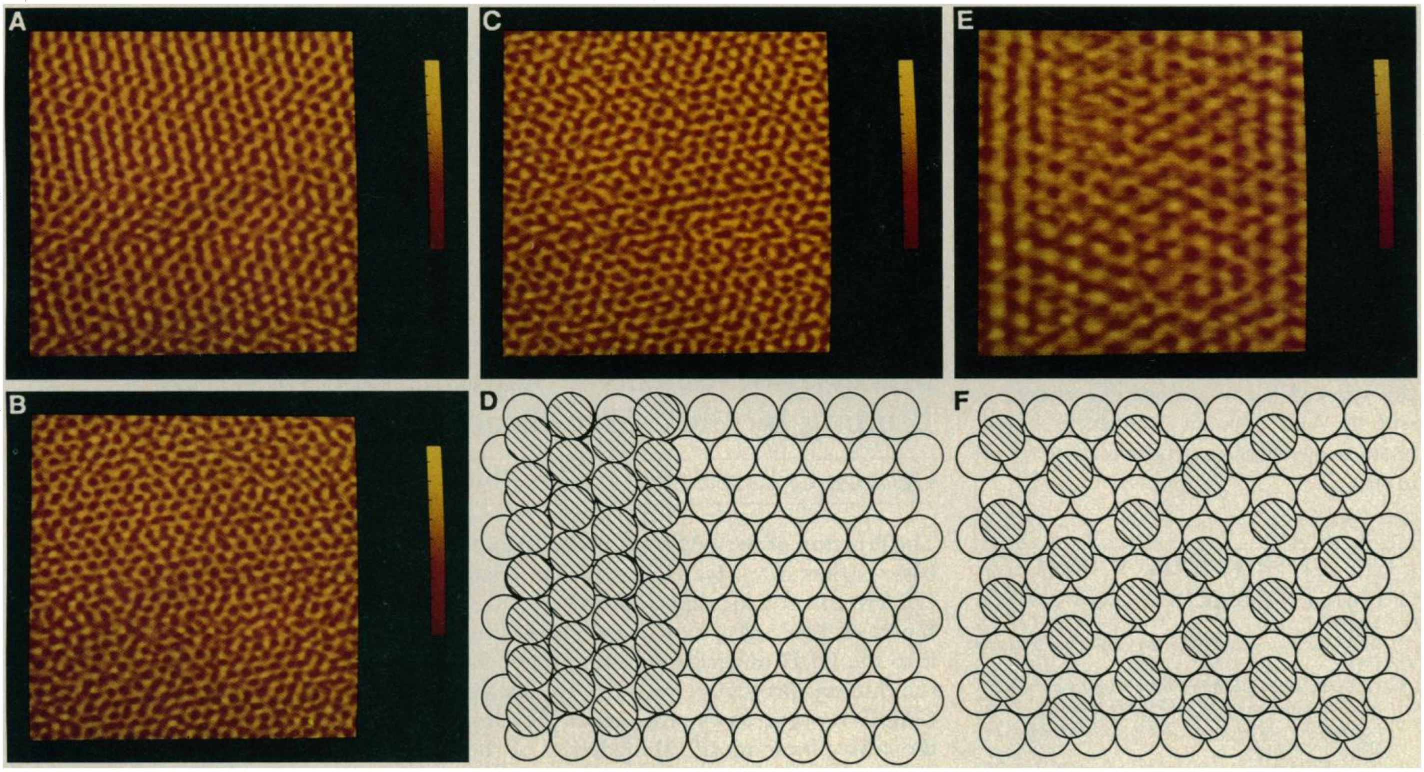

Fig. 2. AFM images (6 nm by 6 nm) of a Au(111) electrode surface in electrolyte + 10^{-3} M Cu^{2+} under potential control at different voltages. (**A**) $V = +0.7$ V showing Au(111) corrugation. (**B**) Bulk-deposited Cu at −0.1 V. The atom-atom distance is 0.26 nm. (**C**) Close-packed overlayer of Cu observed at +0.114 V in 0.1 M perchloric acid. The atom-atom distance is 0.29 nm (**D**) Schematic of incommensurate close-packed overlayer of Cu on Au. The open circles represent Au atoms, while the striped circles represent the Cu. Only part of the monolayer is exhibited in order to demonstrate the overlayer-underlayer orientation. (**E**) $(\sqrt{3} \times \sqrt{3})R30°$ overlayer of Cu on Au observed at +0.144 V in 0.1 M sulfate. Atom-atom distance is 0.49 nm. (**F**) Schematic representing $(\sqrt{3} \times \sqrt{3})R30°$ overlayer of Cu (striped circles) on Au (open circles).

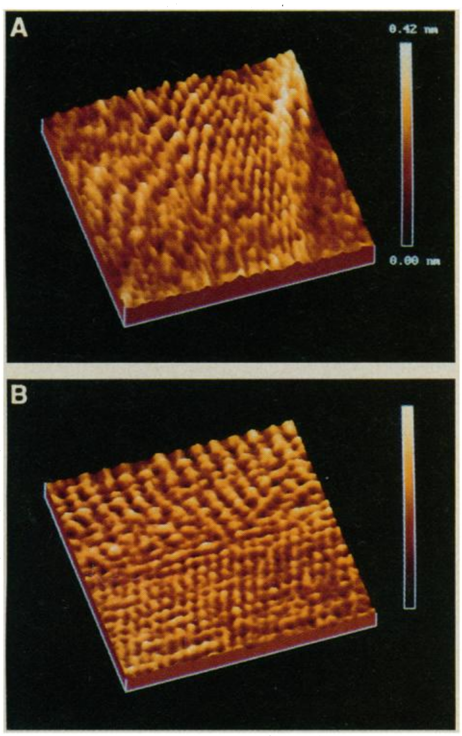

Fig. 3. (**A**) AFM image (6 nm by 6 nm) of bulk Cu dissolution in perchlorate obtained at +0.05 V. A monolayer step is visible in the right of the picture. (**B**) AFM image (6 nm by 6 nm) of a partial submonolayer of Cu on Au in 0.1 M sulfuric acid.

was 0.18 ± 0.05 nm with the Au surface lower than the Cu overlayer. This is direct evidence that only the first monolayer was imaged in these experiments and also provides confirmation of the 30° rotation of the Cu overlayer relative to the Au substrate. It is significant that the underlying surface is Au(111) because that implies that factors other than the immediate local potential gradient normal to the surface must influence the upd process. Large areas of our surface exhibit Au(111) corrugation, but long-range scans show the commonly observed (*22*) "rolling hill" features, which suggests exposure of other Au faces. We did not observe a partial monolayer in perchlorate electrolyte; the close match of the overlayer and substrate lattices makes observation difficult.

At first glance, Fig. 3B appears to be showing the boundary between a partial monolayer of Cu and the Au substrate. It may be, however, that it is really showing a time sequence in which the area starts covered with Cu, which then leaves during imaging to reveal the Au substrate. While more experiments will be necessary to decide unambiguously between these two possibilities, both are consistent with the idea that long-range effects on the surface must influence the upd process.

This study provides important insight into the mechanism of upd in sulfate and perchlorate electrolytes. It is apparent that a change in the electrolyte can strongly affect both the structure and energetics of the upd overlayer. The Cu structure obtained in sulfate is substantially more open than that obtained in perchlorate. One possible explanation for this difference is coadsorbtion of sulfate anions with the Cu. Radiochemical data suggest that prior to Cu upd on Au, there is little or no sulfate on the surface, but that immediately following initiation of this process, substantial sulfate adsorption occurs (*17*). In perchlorate, the close-packed structure does not allow for electrolyte coadsorbtion. Energetically, the observation that Cu upd in perchlorate occurs at potentials ~110 mV more positive than the same process in sulfate suggests that the Cu–Au bond is weaker in sulfate. Partial charge transfer to coadsorbed sulfate in the $(\sqrt{3} \times \sqrt{3})R30°$ overlayer structure could account for this observation, as ionic interactions between adatom and substrate are thought to account for most of the bond strength in these systems (*23*). It is significant that the $Cu^{2+/0}$ redox couple occurs between 40 and 170 mV more positive in perchlorate relative to sulfate (*24*), a result that would again suggest stabilization of Cu^{2+} in dilute sulfuric acid. This may in part derive from the substantially higher pK_a (acidic constant) of perchloric acid (-10) relative to sulfate (-2).

In summary, we observed a complete adsorption and desorption cycle for a metal onto another metal surface with atomic resolution. In the Cu on Au(111) system, the electrolyte plays a major role in determining the structure of the upd monolayer, a result that can be explained by the degree of charge transfer between coadsorbed Cu and electrolyte. The atomic resolution obtained on close-packed metal surfaces in electrolyte with the AFM makes it a valuable technique in studying other electrochemical processes in situ.

REFERENCES AND NOTES

1. G. Binnig, C. F. Quate, Ch. Gerber, *Phys. Rev. Lett.* **12**, 930 (1986).
2. K. Wickramasinghe, *Sci. Am.* **260**, 98 (October 1989).
3. D. Kolb, in *Advances in Electrochemistry and Electrochemical Engineering*, H. Gerisher and C. Tobias, Eds. (Wiley, New York, 1984), vol. 11, pp. 125–271.
4. R. Adzic, *ibid.*, vol. 13, pp. 154–260.
5. Y. Nakai, M. S. Zei, D. M. Kolb, G. Lehmpfuhl, *Ber. Bunsenges. Phys. Chem.* **88**, 340 (1984).
6. O. R. Melroy *et al.*, *Langmuir* **4**, 728 (1988).
7. O. M. Magnussen, J. Hotlos, R. J. Nichols, D. M. Kolb, R. J. Behm, *Phys. Rev. Lett.* **64**, 2929 (1990).
8. Digital Instruments, Inc., 6780 Cortona Drive, Santa Barbara, CA 93117.
9. B. Drake *et al.*, *Science* **243**, 1586 (1989); S. Alexander *et al.*, *J. Appl. Phys.* **65**, 164 (1989); G. Meyer and N. M. Amer, *Appl. Phys. Lett.* **53**, 1045 (1988).
10. We used microfabricated cantilevers (*11*) which were commercially available with integrated tips (*12*). Data acquisition rates were 5 seconds per image with an operating force of $\sim 10^{-8}$ N between tip and sample.
11. T. R. Albrecht and C. F. Quate, *J. Vac. Sci. Technol. A* 6, 271 (1988).
12. Park Scientific Instruments, 476 Ellis Street, Mountain View, CA 94043.
13. A Cu wire, in contact with the perchlorate electrolyte at the fluid outlet, served as the reference electrode, and all voltages were referred to this wire. The counterelectrode was a stainless-steel spring clip that also held the AFM cantilever in place. The working electrode was a 100-nm-thick Au film evaporated onto mica with an exposed electrode area of 0.32 cm^2. Reagent grade $HClO_4$, H_2SO_4, $Cu(ClO_4)_2 \cdot 6H_2O$, and $CuSO_4 \cdot 5H_2O$ and water from a Millipore-Q purifier were used. Solutions (10^{-3} M in Cu) were not deoxygenated prior to use. Potential control was obtained with a Bioanalytical Systems CV-1B potentiostat.
14. M. S. Zei, G. Qiao, G. Lehmpfuhl, D. M. Kolb, *Ber. Bunsenges, Phys. Chem.* **91**, 349 (1987).
15. In our sample cell, desorption peaks were not as distinct as those reported by other authors [J. W. Schultz and D. Dickertmann, *Surf. Sci.* **54**, 489 (1976)] on true single-crystal electrodes. This may be a manifestation of our somewhat rougher surface or may reflect interference arising from the stainless-steel counter electrode. However, the underpotential shifts and overall appearance of the current-voltage curves were the same as in cells where a Pt wire was used as the auxiliary electrode.
16. S. Manne, H.-J. Butt, S. A. C. Gould, P. K. Hansma, *Appl. Phys. Lett.* **56**, 1758 (1990).
17. G. Horanyi, E. M. Rizmayer, P. Joo, *J. Electroanal. Chem.* **152**, 211 (1983).
18. P. Zelenay, L. M. Rice-Jackson, A. Wieckowski, *ibid.* **283**, 389 (1990).
19. J. Weichers, T. Twomey, D. M. Kolb, R. J. Behm, *ibid.* **248**, 451 (1988).
20. P. H. Lippel. R. J. Wilson, M. D. Miller, Ch. Woll, S. Chiang, *Phys. Rev. Lett.* **62**, 171 (1989).
21. We found that this rotation relative to the Au(111) lattice was unchanged whether we compared with the Au surface before or after Cu deposition and stripping. The orientation of the Au lattice did not change during the course of the experiment.
22. J. Schneir *et al.*, *J. Appl. Phys.* **63**, 717 (1988).
23. J. D. Levine and E. P. Gyftopoulos, *Surf. Sci.* **1**, 171 (1964).
24. U. Bertocci and D. R. Turner, in *Encyclopedia of Electrochemistry of the Elements*, A. J. Bard, Ed. (Dekkar, New York, 1974), vol. 2, chap. 6.
25. We thank S. A. C. Gould and S. Hansma for help with the image processing. Supported by National Science Foundation grant DMR-8917164 (S.M. and P.K.H.) and by Presidential Young Investigator Award CHE-9057953 (A.A.G.).

27 July 1990; accepted 19 October 1990

Methylation-Sensitive Sequence-Specific DNA Binding by the c-Myc Basic Region

George C. Prendergast and Edward B. Ziff

The function of the c-Myc oncoprotein and its role in cell growth control is unclear. A basic region of c-Myc is structurally related to the basic motifs of helix-loop-helix (HLH) and leucine zipper proteins, which provide sequence-specific DNA binding function. The c-Myc basic region was tested for its ability to bind DNA by attaching it to the HLH dimerization interface of the E12 enhancer binding factor. Dimers of the chimeric protein, termed E6, specifically bound an E box element (GGCCACGTGACC) recognized by other HLH proteins in a manner dependent on the integrity of the c-Myc basic motif. Methylation of the core CpG in the E box recognition site specifically inhibited binding by E6, but not by two other HLH proteins. Expression of E6 (but not an E6 DNA binding mutant) suppressed the ability of c-*myc* to cooperate with H-*ras* in a rat embryo fibroblast transformation assay, suggesting that the DNA recognition specificity of E6 is related to that of c-Myc in vivo.

THE BASIC REGIONS IMMEDIATELY NH$_2$-terminal to the oligomerization domains in HLH and leucine zipper proteins specifically recognize DNA with high affinity when assembled into functional dimers (*1–8*). c-Myc, a nuclear protein with unknown function, has a region rich in basic amino acids adjacent to a HLH domain (*1*), suggesting that it is a sequence-specific DNA binding protein. We sought to determine the DNA sequence recognized by the c-Myc basic region. To present the c-Myc basic region to DNA in a dimeric form, we constructed a chimeric protein that contained the dimerization interface of E12, an enhancer binding protein (*2*). The chimeric protein, termed E6, is a NH$_2$- and COOH-terminal truncated form of E12 (*9*), which exchanged the c-Myc basic motif for the corresponding E12 sequence (Fig. 1).

Similarity between the basic motifs of c-Myc and the putative HLH protein transcription factor E-3 (TFE-3) suggested that they might recognize similar DNA sequence elements (*10*). Therefore, a gel mobility shift assay was used to monitor binding of the E6 protein to ^{32}P-labeled oligonucleotide probes that contained either the μE3 E box site from the immunoglobulin heavy chain enhancer or the upstream stimulatory factor (USF) E box site from the adenovirus major late promoter, both of which are recognized by TFE-3 (*10*). We used TFE-3 as a positive control for binding. No complex was observed upon incubation of E6 with the μE3 E box probe (E$_{\mu E3}$); however, a strong complex was observed with the USF E box oligonucleotide probe (E$_{USF}$), whose formation was competed by unlabeled cognate oligonucleotide (Fig. 2A). We find that, as expected, neither intact E12 nor a truncated form of E12 that corresponded to the part of the protein found in the E6 construct bound the E$_{\mu E3}$ or E$_{USF}$ oligonucleotide probes (*11*).

To show that E6 bound E$_{USF}$ as a dimer through the c-Myc basic motifs, additional constructs were tested (Fig. 1). Gel fractionation of complexes formed between E$_{USF}$ and cotranslation products of E6 and E6Δ, [a $\sim$10-kilodalton protein that lacked 184 amino acids of the E6 NH$_2$-terminus] showed complexes of intermediate mobility relative to E6 or E6Δ alone (*11*). The appearance of intermediate mobility bands is consistent with the formation of E6-E6Δ dimers. In order to determine whether the integrity of the c-Myc basic motif was required for E$_{USF}$ binding, the E6mutN, E6mutB2Q, and E6mutR mutants were generated (Fig. 1). Equivalent amounts of protein, as judged by SDS–polyacrylamide gel quantitation, were tested for binding to

Howard Hughes Medical Institute, Department of Biochemistry, and Kaplan Cancer Center, New York University Medical School, New York, NY 10016.